Seamounts control subducted carbonate recycling in Central America – evidence from stable Sr isotopes

Alexander J. Hammerstrom*[1,2], Rita Parai[2], Richard W. Carlson[3], Stephen J. Turner[4]

[1] Department Earth, Geographic, and Climate Sciences, University of Massachusetts Amherst, Amherst, MA; ahammerstrom@umass.edu [Corresponding Author]

[2] Department of Earth and Planetary Sciences, Washington University in St. Louis, St. Louis, MO; parai@wustl.edu

[3] Carnegie Institution for Science Earth and Planets Laboratory, Washington D.C.; rcarlson@carnegiescience.edu

[4] Department of Earth and Atmospheric Sciences, University of Houston, Houston, TX; sjturner4@uh.edu

Seamounts control subducted carbonate recycling in Central America – evidence from stable Sr isotopes

Alexnder J. Hammerstrom*, Rita Parai, Richard W. Carlson , Stephen J. Turner

Abstract

Accurate estimates of carbon recycling efficiency at subduction zones are crucial for understanding the long-term evolution of the planet's climate. Estimating subducting carbon recycling efficiency is difficult, however, due to magmatic degassing deep within the crust. Stable strontium (δ^{88}Sr) isotopes have the potential to serve as an additional proxy for carbonate recycling due to carbonate's high Sr concentrations and unique δ^{88}Sr composition. New data from Nicaraguan lavas and sediments verify that Sr can indeed be used to track subducting carbon. When interpreted in conjunction with other magmatic trace element abundances, these data reveal systematic variations that are best understood as the effects of seamount subduction. Seamounts erupting at the same time carbonate-dominated sedimentation ceased on the Cocos plate could potentially 'cap' the carbonate layer and control the degree to which carbonate material is transported to the arc. This model can also be used to quantify the flux of carbonate sediment from the slab to the arc and thus provides an independent method to estimate the magmatic carbon recycling efficiency for the Nicaraguan Arc. Our model shows, absent seamounts, 26% to 52% of carbon from subducted carbonate is returned to the arc, an estimate consistent with recent estimates made from volcanic gases.

Introduction

Carbon cycling in subduction zones has played a key role in maintaining the planet's climate and long-term habitability[1-5]. Some fraction of the carbon initially subducted is quickly returned to the surface through volcanic arcs, with the remainder transported to the deep mantle. The proportion of initially subducted carbon that is returned from the slab to arc is often referred to as the "carbon recycling efficiency." Though accurate estimates of the carbon recycling efficiencies of volcanic arcs are essential to our understanding of Earth's planetary evolution, recent estimates range widely, from 14% to 100%[1,6-19]. This range persists largely because arc magmas lose most of their initial carbon budget to degassing deep in the crust. Even melt-inclusions hosted in primitive olivines likely sample liquids that have lost CO_2 prior to entrapment[20]. As such, direct sampling of the primary arc magma carbon concentrations or isotope ratios may not be possible in most cases.

Most estimates of carbon recycling efficiency are instead derived from measurements of CO_2 abundances and/or isotope ratios of volcanic gases[9-11,13], which also have limitations. For example, carbon fluxes at volcanic arcs are spatially and temporally variable, and the extent of diffuse degassing is not usually well constrained[10-12,19]. Carbon isotopes can also fractionate during slab devolatilization and volcanic degassing[21], crustal contamination, and shallow processes such as calcite precipitation in the forearc[11].

Here, we investigate the potential of Sr stable isotope ratios as a tracer of carbonate recycling from a subducting slab to a volcanic arc using high-precision double-spike stable Sr isotope (Sr isotope data are reported as $^{88}Sr/^{86}Sr$ in standard delta notation, relative to NIST SRM-987 in units of permil as: $\delta^{88}Sr$ (‰)= $[(^{88}Sr/^{86}Sr)_{sample}/(^{88}Sr/^{86}Sr)_{SRM987} - 1] \times 1000$) and radiogenic $^{87}Sr/^{86}Sr$ measurements of Cocos plate sediments and arc lavas from Telica, Cerro Negro, and Masaya volcanoes in the Nicaraguan segment of the Central American Volcanic Arc. These Sr isotope data, in conjunction with traditional radiogenic isotopes and trace element abundances, provide a novel way to quantify carbon recycling efficiency. Our results also motivate a re-evaluation of the origins of geochemical variability present among Central American arc lavas, which appears to be importantly regulated by subducting seamounts.

The Central American Volcanic Arc (Fig. 1a) extends ~1400 km from the Mexico-Guatemala boarder to Panama, where the Cocos Plate subducts underneath the Caribbean at a rate of 5.6 - 6.4 cm/yr[22]. The subducting plate consists of 20 Ma oceanic crust produced at the East Pacific Rise and carries numerous seamounts with elevations up to 2000 m above the seafloor and diameters of up to 14 km[23]. The ocean floor offshore of Central America is covered by two sediment packages of similar thickness: an upper hemiplegic unit and a lower unit dominated by pelagic carbonate (Fig. 2a and b)[24-28]. The mid-Miocene carbonate crash led to a rapid shift in sediment composition between these layers[29]. Cores from Deep Sea Drilling Program site 495 off Guatemala and Ocean Drilling Program site 1039 off the Nicoya Peninsula of Costa Rica (Fig. 1a) show that the sediments remain uniform in thickness and distribution along the entire length of the arc[26,30].

As with all arc-front stratovolcano lavas, the volcanic rocks of the Central American volcanic front inherited the distinct geochemical signatures of subducted materials. Studies of the Northern Guatemala-El Salvador[28] and Southern Costa Rica-Panama[31,32] segments have also identified isotope compositions that appear to originate from the lithospheric mantle and the Galapagos hotspots, respectively. The volcanic rocks of Nicaraguan segment, by contrast, mostly reflect a depleted MORB mantle (DMM) source overprinted with the incompatible trace element pattern of a typical arc lava (e.g. enrichment of Rb, Ba, Th, U, Pb, and Sr and depletion in Nb, Ta)[26]. The upper plate of the Nicaraguan segment is thin and mostly oceanic in origin with little evidence for crustal assimilation[33]. A comparison between thermo-mechanical models of the slab beneath Nicaragua and experimentally determined solidus temperatures[34,35] (Fig. 1b) indicates that at least the upper 1 km of the slab reaches temperatures that exceed the H_2O-saturated solidi for carbonate and pelitic sediments[35-37], altered oceanic crust (AOC)[38], and unaltered MORB[39]. A similar comparison shows that progressive lawsonite dehydration in the lower slab layers should provide a continuous source of water to the slab top (Fig. 1b)[35]. This suggests that hydrous slab melting is the dominant process by which subducting materials are transferred to the mantle wedge in the Nicaraguan segment, and that carbonate melting may mediate the CO_2 flux from the slab to the arc.

Our current understanding of carbon fluxes out of the Central American arc are mostly derived from measurements of volcanic gases and fluid seeps. Most estimates of arc CO_2 fluxes utilize direct measurements of fumarole $CO_2/^3He$ or CO_2/SO_2 alongside an assumed ^3He flux or an independently measured SO_2 flux. Using this approach, Shaw et al. (2003) estimated that the carbon flux from Costa Rican and Nicaraguan arc segments accounted for only ~15% of the total subducting carbon budget. Carbon fluxes estimated by Mather et al. (2006) and Aiuppa (2014) are similar to that of Shaw (2003), while de Moor et al. (2017)'s study of carbon outgassing from 2015-2016 are much higher, indicating carbon recycling efficiencies as high as ~76%. The increased carbon recycling efficiency estimate of de Moor et al. (2017) could be due to improved methodology and much denser sampling, but also coincided with a net increase in volcanic activity during their study period. This suggests that arc CO_2 fluxes can be highly variable across years-long timescales. Recent work by Barry et al. (2019) measured deeply sourced hot springs along two across-arc transects in Costa Rica and estimated that an additional ~19% of subducted carbon may be lost from the slab beneath the forearc. Their total slab-derived carbon outputs are consistent with recent global carbon recycling efficiency estimates of 46%-65%[8,15].

Helium and carbon isotope ratios in gas samples can also be used to determine the relative contributions of subducting materials to the overall carbon budget of arcs. Isotope studies of Central American gases largely agree that most of the carbon emitted through the arc originates from subducting carbonate[9,40,41], consistent with the fact that the sedimentary carbonate layer dominates the carbon budget of the subducting slab.

Trace element abundances in Central American lavas serve as additional proxies for carbonate and hemipelagic sediment recycling from the slab to the arc[26]. This is possible because the hemipelagic sediment has high concentrations of most incompatible trace elements, while the carbonate layer is diluted in most trace elements aside from Sr, Ba, La, and Pb (Fig. 2a), leading to distinct downcore variations in trace element ratios such as Ba/Th and U/La (Fig. 2b). Central American arc lavas exhibit correlated variations in Ba/Th and U/La, presumably due to varying recycling efficiencies of these sediment layers. In some arcs, these ratios could be controlled by the addition of aqueous fluids from the slab, which fractionate ‘fluid mobile’ elements such as Ba and U from ‘fluid immobile’ elements such as Th and La[42]. The negative correlation between these ratios among Nicaraguan lavas (Fig. 3) is inconsistent with aqueous fluid control for the Nicaraguan arc, however, and accords well with variance expected for contributions from the different sediments. The hypothesis that the incompatible trace element compositions of these lavas are controlled by variable subducting sediment compositions is further confirmed by a correlation[43] between U/La and $^{10}Be/^{9}Be$[33,44].

These trace element proxies show that the sediment recycled from the slab to the arc must be highly variable even though core samples all reflect similar offshore sediment profiles. Patino et al. (2000) postulated that this could be due either to off-scraping of the upper hemipelagic sediments from horsts to grabens or to a more complicated multi-stage slab melting process. Others have proposed mechanisms relating to slab dip, differing extents of lithospheric serpentinization, varying extents of fore-arc erosion, or temporal variability in the spatial distribution of the carbonate sediment layer[10,26,29,45].

While the trace element approach has produced important qualitative constraints on sediment recycling in Central America, these proxies cannot be used to accurately quantify the absolute recycling efficiency of either sediment package. For U/La, this is because U decreases significantly down the entire sediment core (Fig. 2b), including within the hemipelagic layer, as the proportion of preserved organic-rich sediments decreases[26,29]. The relationship between Ba/Th in sediments vs lavas is complicated by the fact that Ba concentrations in pore fluids and sediments offshore of Costa Rica indicate that upwards of ~60% of the incoming bulk sediment Ba may be lost to the forearc[46]. Uncertainties such as these make it difficult to directly estimate the recycling efficiencies of the individual sediment layers from trace element data alone.

The high Sr concentrations and distinct Sr isotope compositions of carbonates make Sr stable isotopes a promising proxy for recycled carbonate that is free from the uncertainties inherent in gas data or trace element ratios. Sr^{2+} can readily substitute for Ca^{2+}, leading to elevated Sr abundances in most carbonate-rich marine sediments. Seawater inherits terrigenous Sr with high δ^{88}Sr (0.39‰)[47,48], whereas biogenic marine carbonates are typically a mix of foraminifera and coccoliths with much lower δ^{88}Sr (0.14‰ to 0.27‰; Fig.4)[47,48]. High-precision TIMS measurements of δ^{88}Sr in typical MORB samples are limited, but thus far cluster around 0.28± 0.05‰[49]. Experimental work shows that high-temperature hydrothermal alteration of basalt leads to elevated δ^{88}Sr[50], and while actual AOC δ^{88}Sr measurements are also limited, existing data support this general process[49]. High-temperature magmatic processes, on the other hand, have little effect on Sr isotope fractionation in systems for which Sr behaves as an incompatible element. Plagioclase fractionation may have a small impact on magmatic δ^{88}Sr[51]. The application of Sr to carbonate recycling during subduction also benefits from the fact that Sr and C partition similarly between carbonate and melt[52,53]. Together, these studies show that subducting materials, and marine carbonates in particular, exhibit distinct δ^{88}Sr compositions that should be reflected as recycled components in mafic arc lavas. This proxy has the potential to constrain carbon recycling from measurements of lava samples without the complications that can arise from early carbon degassing and the various processes that can fractionate trace element ratios. Stable Sr isotopic compositions thus could provide an alternative method to estimate long-term carbon fluxes at subduction zones.

Lavas from the Nicaraguan arc were chosen for this study due to their strong sediment signature and lack of evidence for crustal assimilation or influence from the Galapagos plume[28,29,54,55]. Nine samples were selected to encompass the full range of U/La and Ba/Th found among Nicaraguan lavas (Fig. 3). The samples include lavas from Cerro Negro, Masaya, and Telica volcanoes that were obtained from the Rutgers CAVA sample repository[56] and have been previously analyzed for major elements, trace elements, and radiogenic isotopes (Pb, Nd, and some Sr)[26,57]. These prior studies showed that the selected samples exhibit compositional variations that largely reflect slab and mantle processes.

Results

Variation in $^{87}Sr/^{86}Sr$ and $\delta^{88}Sr$ in Central American lavas and sediments

$^{87}Sr/^{86}Sr$ and $\delta^{88}Sr$ data are presented in Table 1 and shown in Figure 5. External precision, reported as the average 2-SE for $\delta^{88}Sr$ values is <0.02‰. Carbonate sediment $\delta^{88}Sr$ ranges from 0.170±0.016‰ to 0.219±0.016‰, consistent with the calcareous Aegean sediments ($\delta^{88}Sr$=0.195‰ to 0.213‰) measured by Klaver et al. (2020). Surprisingly, the hemipelagic sediment sample is isotopically lighter ($\delta^{88}Sr$=0.146‰±0.021‰) than the carbonate, which suggests that the Sr budget of the hemipelagic sediments is also dominated by biogenic material. Both sediments have $^{87}Sr/^{86}Sr$ ratios near that of modern seawater (~0.709), consistent with Patino et al. (2000). Nicaraguan arc lavas ($\delta^{88}Sr$=0.212±0.013‰ to 0.322±0.015‰) exhibit a greater relative variation in $\delta^{88}Sr$ than the sediments. Samples from Masaya and Cerro Negro define heavy and light $\delta^{88}Sr$ end members, respectively, while Telica $\delta^{88}Sr$ varies between the two (0.243±0.014‰ to 0.279±0.019‰). Arc lava $^{87}Sr/^{86}Sr$ ratios (0.7040 to 0.70419) are uniform relative to the range of subducting materials and have compositions closer to DMM or AOC than sediments (Fig. 5). The altered ocean crust composite samples ($\delta^{88}Sr$=0.247±0.008‰ to 0.263±0.014‰; $^{87}Sr/^{86}Sr$ = 0.70330 to 0.70679) are consistent within uncertainty to measurements of the same samples by Klaver et al. (2020) but are unlikely to represent the compositional range of actual subducting ocean crust as discussed in greater detail in the Online Supplement.

δ^{88}Sr provides new insights into Nicaraguan subduction dynamics

The primary goal of this study was to assess stable Sr isotopic variability as a proxy for carbonate recycling at subduction zones, but these data also shed new light on important subduction zone systematics that directly influence the geochemical variability of Nicaraguan arc magmas. Because the hemipelagic and carbonate sediment packages both have low δ^{88}Sr, and because the arc data unexpectedly span a larger range in δ^{88}Sr than the subducting sediments, a robust estimate of sediment recycling efficiencies requires interpretations of Sr isotope data alongside other trace element compositions. To quantify the provenance of Sr erupted in the arc, we first employ a simple Sr mass balance utilizing trace element abundances and ^{87}Sr/^{86}Sr data. This approach can determine the general proportion of Sr in the arc lavas originating from all sediments, AOC, and mantle. Next, we incorporate the δ^{88}Sr data to distinguish between the inputs of the carbonate vs hemipelagic sediment. These constraints indicate that Nicaraguan arc lavas require both a high-δ^{88}Sr altered ocean crust component and an unaltered crustal component with low-δ^{88}Sr. We propose that these combined signals may result from the subduction of seamounts along the Cocos plate, and present an internally consistent, quantitative model that supports this hypothesis. This model can also be used to quantify the flux of carbonate sediment from the slab to the arc and thus provides an independent method to estimate the magmatic carbon recycling efficiency for the Nicaraguan Arc.

Quantifying strontium sources from sediment, AOC, and the ambient mantle

The fact that the arc lava $^{87}Sr/^{86}Sr$ data lie much closer to the DMM and AOC compositions than the sediments (Fig. 5) means that the Sr budget of the arc lavas is dominated by Sr from sources with MORB- or AOC-like $^{87}Sr/^{86}Sr$. This suggests that the $\delta^{88}Sr$ variability of the arc lavas is at least partially inherited from $\delta^{88}Sr$ variability among ambient mantle or mafic crustal sources that have low $^{87}Sr/^{86}Sr$, rather than sediments. For example, the high $\delta^{88}Sr$ and moderate $^{87}Sr/^{86}Sr$ possibly are inherited from AOC, whereas low $\delta^{88}Sr$ and DMM-like $^{87}Sr/^{86}Sr$ are contributed from the ambient mantle. Alternatively, the low $^{87}Sr/^{86}Sr$ could be inherited from the subducting basaltic crust, which itself may have variable $\delta^{88}Sr$.

A conventional mass balance using trace element ratios and $^{87}Sr/^{86}Sr$ demonstrates that the Sr contribution from the subducting slab far outweighs Sr inherited from the ambient mantle, however, and instead supports a model with varied $\delta^{88}Sr$ inherited from the subducting ocean crust. The thermal model in Figure 1b shows that the slab surface temperatures significantly exceed the hydrous solidi of all subducting lithologies, while lawsonite dehydration in the lower portions of the slab should provide a consistent source of H_2O. Our mass balance calculation makes use of published AOC hydrous melt compositions and sediment melt partition coefficients[58], though with $DSr^{carbonate/melt}=1$[53]. As shown on Figure 6a, adding slab melt (either sediment or AOC melt) to the DMM leads to a rapid drop in Sr/Yb, because Yb is retained by residual garnet in the slab. To reach the Sr/Yb composition of the arc requires ~7%-15% total slab melt addition. The amount of sediment melt in the mantle source is then quantitatively constrained by $^{87}Sr/^{86}Sr$ to be <2% carbonate melt or <4% hemipelagic sediment melt, while the amount of AOC melt is between 6% and 13% (Fig. 6a). This mass balance shows that only ~10% of the Sr in the arc lavas could have originated from the ambient mantle.

Because very little of the Sr in erupted arc lavas is derived from the ambient mantle, the ambient mantle source has a negligible influence on δ^{88}Sr. An alternative low-δ^{88}Sr, low-^{87}Sr/^{86}Sr reservoir is thus required from the slab. This is depicted quantitively by the two mixing triangles on Figure 6b. The first (blue) mixing triangle spans between hemipelagic sediment, carbonate sediment, and a hypothetical AOC melt composition with δ^{88}Sr =0.36‰ (consistent with experimental data[50], and discussed in more detailed in the Online Supplement), which is the minimum AOC value capable of producing a mixing triangle that overlaps the composition of Cerro Negro, the high δ^{88}Sr arc end member. For the second (gray) mixing triangle, the pure AOC melt end member is replaced by a mixture of 94% DMM and 6% AOC melt, which is the minimum possible AOC melt addition inferred from figure 6a. Varying the influence of the DMM within this allowable range on figure 6b does not significantly shift the position of the mixing triangle, and neither triangle overlaps the remainder of the arc data. To account for the full range of the arc data, there must instead be an additional slab component with both low ^{87}Sr/^{86}Sr and low δ^{88}Sr. Figure 6c shows that a second ocean crust component with a δ^{88}Sr equal to average unaltered MORB (δ^{88}Sr =0.28± 0.05‰)[49] could plausibly serve as this additional slab component. In this case, the high δ^{88}Sr composition of Cerro Negro would reflect a large contribution of AOC melt, while the low-δ^{88}Sr composition of Masaya would be dominated by a melt of unaltered ocean crust.

To summarize, the arc lava Sr budget is dominated by low-^{87}Sr/^{86}Sr sources that must have variable δ^{88}Sr. Mass balance shows that the low-δ^{88}Sr, low-^{87}Sr/^{86}Sr source cannot be the

DMM. Instead, two distinct ocean crust components are needed to account for the full range of arc lava δ^{88}Sr. The Cerro Negro lava end member requires an AOC melt with a δ^{88}Sr >0.36‰ whereas the Masaya end member must have an ocean crust component with δ^{88}Sr <0.28‰. We propose that this second low-^{87}Sr/^{86}Sr, low-δ^{88}Sr component represents oceanic crust with an unaltered MORB composition.

Evidence for co-variation of ocean crust and sediment components

A surprising result is that the proportions of high-δ^{88}Sr vs low-δ^{88}Sr ocean crust appear to co-vary with the proportions of hemipelagic and carbonate sediment. Figure 6c shows that a low-δ^{88}Sr, DMM-like, ocean crust component (gray hexagon) produces an ocean crust-sediment mixing triangle that overlaps the compositions of the Telica (gray triangles) and Masaya (red diamond) samples but does not encompass the composition of the Cerro Negro (blue circle). An alternative mixing triangle starting from a high-δ^{88}Sr AOC is required to account for the Cerro Negro composition, but it does not encompass any other samples. The Cerro Negro composition is reproduced within uncertainty by a mixture of high-δ^{88}Sr AOC and a range of different sediment proportions, though other trace element constraints (e.g., Fig. 3) suggest that a dominantly hemipelagic sediment component is implausible for this volcano. In contrast, the composition of the Masaya end member can only be reproduced using the low-δ^{88}Sr ocean crust component and a sediment that is almost entirely dominated by the hemipelagic component. The Masaya composition thus requires a dominantly hemipelagic sediment and less altered oceanic crust, while the Cerro Negro composition requires high-δ^{88}Sr altered oceanic crust and a greater contribution from carbonate sediment.

Plausible quantitative mixing scenarios for these two end members are shown on Figure 6d. Mixing between an AOC melt with δ^{88}Sr = ~0.36‰ and a sediment melt composed of 70% carbonate and 30% hemipelagic sediment (Mixing Scenario A, Fig. 6d) is consistent with the composition of Cerro Negro. Sediment proportions in Scenario A are based on the relative masses of each sediment layer observed on the modern Cocos plate. A more complete solution assumes 9% Sr from AOC melt (pink cross, Fig. 6d). There is no solution using either of these sediment or ocean crust compositions, however, that is consistent with the composition of Masaya. A successful Masaya model instead requires an ocean crust component with δ^{88}Sr~NMORB (0.28‰) and a sediment melt containing <5% carbonate material (Mixing Scenario B, Fig. 7d; or blue cross, which includes 7.5% Sr from AOC melt).

These new constraints from δ^{88}Sr measurements and our models raise three primary questions, (1) What is the source of the second low-δ^{88}Sr ocean crust component? (2) Why is Masaya less impacted by carbonate sediment? And (3) What causes the sediment proportions and ocean crust compositions to vary simultaneously?

Covariations in slab melt compositions driven by seamount subduction

The numerous seamounts on top of the Cocos plate offshore of Nicaragua (Fig. 1a) provide a plausible source for the low-δ^{88}Sr ocean crust component and may also regulate carbonate recycling from the slab to the arc. Herbich et al. (2015) found that these seamounts erupted from 22.4 Ma to 7 Ma and that most have low ^{87}Sr/^{86}Sr compositions (^{87}Sr/^{86}Sr<0.703), from which we infer they likely have NMORB-like δ^{88}Sr. Seamounts erupted after 11 Ma –

which post-date the “carbonate crash”[29] – could potentially ‘cap’ the carbonate layer and prevent the transfer of carbonate material from the slab to the mantle wedge.

The seamounts provide a reasonable explanation for why samples that mix to the low-δ^{88}Sr ocean crust component also require a smaller contribution from subducting carbonate (e.g., Fig. 6c-d). Absent seamounts, the down-going slab surface consists of typical AOC overlain by a carbonate and hemipelagic sediment (Fig. 7a), in which case melts of the upper slab would be a mixture of typical AOC and carbonate+hemipelagic sediment in proportions comparable to the total subducting sediment masses. This scenario accounts best for the end-member composition of Cerro Negro (Mixing Scenario A, Fig. 6d). If a seamount erupted following the carbonate crash, however, it would cap the carbonate layer and become blanketed in hemipelagic sediment prior to subduction (Fig. 7b). In this case, the slab melts would be a mixture of depleted and less-altered seamount material combined with hemipelagic sediment, consistent with the end-member composition of Masaya (Mixing Scenario B, Fig. 6d).

Intermediate scenarios are also possible. Older seamounts erupted prior to the carbonate crash could produce slab melts composed of depleted ocean crust and varying proportions of hemipelagic and carbonate sediment (Fig. 7c). Alternatively, where the subducting plate is capped by thinner outlying seamount lava flows, melting might affect both high- and low-δ^{88}Sr ocean crust alongside both sediment units (Fig. 7d). Either of these intermediate scenarios might account for the range of compositions observed among the Telica samples.

Testing the seamount hypothesis with quantitative trace element modeling

If the Sr isotope variations of the arc lavas reflect changing sediment proportions due to the presence of seamounts on the subducting plate, then systematic compositional differences in a variety of trace element abundances should also be observed. To evaluate this hypothesis, we first consider the Th/Nd ratio, which is sensitive to hemipelagic sediment input. Mixing model component compositions in Figure 8 are based on the same sources as those in Figure 6. Figures 8a-b show that the mixing scenarios determined from Sr isotope constraints are also successful for Th/Nd: Mixing Scenario A, which includes a bulk sediment mixture comparable to total subducting sediment along with typical AOC, produces a sediment mixing curve that passes through the lower Th/Nd of Cerro Negro. Mixing Scenario B, which is dominated by hemipelagic sediment and melt from unaltered ocean crust, produces a mixing curve that passes through the higher Th/Nd composition of Masaya. The same parameters used in the preferred Masaya and Cerro Negro quantitative models based on Sr isotopes alone (Fig. 6) also reproduce these volcano Th/Nd compositions (Fig. 8a-b).

Though it is difficult to distinguish between the two ocean-crust end member components on figure 8a and b, Th/Nd ratios clearly show that the high-δ^{88}Sr and low-δ^{88}Sr lavas of Cerro Negro and Masaya, respectively, require significantly different sediment inputs consistent with the proportions determined by Sr isotope constraints (Fig. 6d). Masaya lavas require little to no carbonate input and a low-δ^{88}Sr, DMM-like, unaltered ocean crust whereas Cerro Negro can be explained by mixing between a sediment melt with a ~70% carbonate component and a high-δ^{88}Sr AOC.

A further test of this conceptual model can be conducted using the full array of commonly measured incompatible trace element abundances. Figure 9 shows that after accounting for differences in fractional crystallization and extents of mantle melting, the end member mixing scenarios developed using only Sr isotope ratios (Fig. 6) and Th/Nd (Fig. 8) also reproduce the full array of trace element abundances for both Masaya and Cerro Negro. All elements that are strongly controlled by the slab exhibit a close match in our model except for Ba (dotted lines and open symbols in Fig. 9). A possible mechanism to reconcile the Ba mismatch is the partial loss of Ba from the sediments into the forearc before reaching sub arc depths, as observed in Costa Rica by Solomon and Kastner (2012). The Ba abundances of both Masaya and Cerro Negro can both be reproduced by the model if 50% to 60% of Ba is lost from the hemipelagic sediment prior to subduction (solid lines and closed symbols in Fig. 9). Model results consistent with measured arc lava trace element abundances support our proposed seamount subduction model based on the Sr stable isotope data. This new geochemical framework provides a first-order explanation for the longstanding observation of variable sediment recycling in Central America that was previously not well understood. Additionally, our model results suggest that Ba in the sediments must be lost to the forearc prior to melting.

Carbon recycling efficiency estimates

The calculated proportions of Sr contributed to the arc can now be used to estimate carbon recycling efficiency. Given ~200 m of subducting carbonate sediment with a density of 1.75 g/cm^3 and a convergence rate of 71.5 km/Ma[22], the subducting CO_2 input into the subduction zone from carbonate sediment alone is 27 metric tons per day (t/d). To determine how much of this CO_2 is recycled back to the arc, we take advantage of the fact that experimental water saturated melting Sr and C solid/melt partition coefficients for carbonate[52,53] are both close to unity. Our Sr model (Mixing scenario A, absent seamounts) indicates that the subducting carbonate contributed 48 ppm Sr to the primary arc magmas (compared to ~1500 ppm in the carbonate-rich sediment), which translates to a contribution of ~1.25 wt.% CO_2 to the arc magma (compared to 40% CO_2 in the carbonate-rich sediment). Assuming an eruption rate of rate of ~14 $km^3/Ma/km$[14], the output flux from the arc is therefore between 7 and 14 t/d (based on an intrusive:extrusive ratio of 5-10), which amounts to 26% to 52% of the subducted carbon from carbonate sediment. We note that this estimate of carbon recycling efficiency is specific to carbon initially subducted as carbonate sediment, though as previously noted, this accounts for up to 92% of the total subducting carbon input[10,14]. This result is consistent with the recent estimate for northwestern Costa Rica (~34% to ~46%) from Barry et al. (2019) based on gas measurements. These results thus showcase the potential of a Sr stable isotope proxy based purely on lava compositions to trace magmatic carbon flux in subduction zones.

Discussion

Strontium stable isotope measurements of Nicaraguan arc basalts not only enable direct estimates of magmatic carbon flux from the arc but also shed new light on the subduction zone systematics that give rise to the geochemical variability in Central American arc lavas. $\delta^{88}Sr$ and $^{87}Sr/^{86}Sr$ constraints dictate that (1) in addition to AOC, a second, unaltered, DMM-like crustal component is required to account for the low-δ^{88}Sr lava from Masaya lavas; and (2) co-variation of the ocean crust components with the hemipelagic and carbonate sediment components can account for the full δ^{88}Sr array of the measured Nicaraguan arc lavas. The low-δ^{88}Sr ocean crust component likely comes from subducting seamounts atop the Cocos plate that exhibit mantle-like ^{87}Sr/^{86}Sr. With diameters up to 14 km and elevations up to 2 km above the surrounding seafloor, the seamounts erupted after the carbonate crash plausibly cap the underlying carbonate sediments and AOC producing a “seamount effect” that only allows for the transfer of a hemipelagic+depleted and less-altered seamount material to the arc. End-member mixing proportions for sediment and crustal components are consistent for both Sr isotopes and trace elements. Low-δ^{88}Sr Masaya lavas require mixing of a pure depleted unradiogenic crustal component with a nearly 100% hemipelagic sediment. The high-δ^{88}Sr Cerro Negro end member requires a pure AOC ocean crust component mixing with a sediment component that is ~70% carbonate material. Telica lava δ^{88}Sr values fall between Cerro Negro and Masaya end members and likely were produced by intermediate scenarios that reflect variable proportions of all four components.

Our conceptual model is supported by quantitative forward model results which reproduce the Cerro Negro and Masaya lava end member Sr isotope compositions and most trace element abundances within uncertainty. Using our quantified carbonate flux determined from Sr stable isotope data we estimate that ~26% to ~52% of the carbon from the subducting carbonate sediments is recycled back out of the arc. These estimates are consistent with recent carbon recycling efficiencies from Barry et al. (2019) and Bekaert et al. (2020). The results of this study provide a new quantitative framework to explain the local variations in arc lava geochemistry in Nicaragua and highlight the power of stable Sr isotope compositions as a tool to understand subduction components and carbonate fluxes at arcs. Strontium stable isotopic data have enormous potential to serve as a robust proxy for carbon transfer across subduction zones alongside traditional CO_2 gas and carbon isotope measurements.

Methods

Sample selection

Only samples with Eu*> 0.95 ($Eu/Eu^* = Eu_{cn}/[Sm_{cn} * Gd_{cn}]^{1/2}$) were selected to minimize the potential influence of plagioclase fractionation. Hemipelagic and carbonate sediments from 124 m, 238 m and 362 m core depths recovered from DSDP site 495 were also analyzed to constrain the Sr isotope compositions of the subducting Cocos plate sediments. Two AOC composite powders from Kelly et al. (2003) previously measured for δ^{88}Sr by Klaver et al. (2020) were also analyzed.

Strontium double spike TIMS analysis and sample preparation

Strontium isotope analyses were conducted via Thermal Ionization Mass Spectroscopy (TIMS) using a Sr double-spike to correct for instrumental mass fractionation. Two ~10 mg aliquots of each sample – one containing the Sr double spike and one unspiked – were digested in a 4:1 solution of 16N Aristar Plus trace metal analysis grade HNO_3 and 48N ultra-pure HF in Savillex beakers at 150° C for 48 hours in clean labs at the University of Massachusetts, Amherst. Samples were evaporated to dryness at 100° C then dissolved twice in 20ul of 16N Aristar Plus trace metal analysis grade HNO_3 and evaporated to dryness at 100° C. Following the second dry down, samples were re-digested in 1.5 ml of 8N Aristar Plus trace metal analysis grade HNO_3 for 24 hr at 120° C. Ion exchange chromatography was developed to separate both Rb and Ba from Sr, as the presence of either element has undesirable effects on Sr isotope measurements. For example, eluted Sr solutions with greater than 1 ppm Ba concentrations exhibit deviations of up to 0.8‰ and 0.001 in δ^{88}Sr and ^{87}Sr/^{86}Sr, respectively, compared to ratios measured in pure Sr[59]. Following Sr purification, samples were loaded onto degassed Re filaments along with a TaO_2 activator and measured using a Thermo Finnigan Triton TIMS at the Carnegie Institution for Science Earth and Planets Laboratory in Washington, D.C. (see Online Supplement for additional details).

Forward quantitative modeling approach

The forward trace element and isotopic geochemical model builds off the quantitative framework for global arc lava variations established by Turner and Langmuir (2022c). The goal of this modeling approach is to ascertain the plausibility of a model hypothesis using melting parameters and trace element partition coefficients that are consistent with experimental petrology. The extent of fractional crystallization for the Cerro Negro and Masaya samples were estimated to be 10% and 20%, respectively, using Petrolog modeling software. Extents of mantle melting are estimated from heavy rare earth element abundances. The model uses AOC and sediment melt trace element partition coefficients determined by Turner and Langmuir (2022b).

The ambient mantle was assigned the trace element abundances of the 'DMM' from Workman and Hart (2005), δ^{88}Sr (~0.28‰) that matches the average N-MORB δ^{88}Sr reported by Klaver et al. (2020), and $^{87}Sr/^{86}Sr$ (~0.7028) based on back arc basalts from La Providencia Island[61]. The carbonate sediment composition is based off the weighted average from Patino et al. (2000) for DSDP 495, while the upper hemipelagic sediment composition was re-calculated in bulk to exclude the youngest upper layers, which should not be present on the deeply subducted portion of the slab beneath the arc. For AOC we assume an $^{87}Sr/^{86}Sr$ of 0.7032[58] which is between the average Pacific MORB ($^{87}Sr/^{86}Sr$ = 0.70257)[62] and an upper altered slab layer with $^{87}Sr/^{86}Sr$ equal to ~0.7045[58]. This is based on the observation that alteration processes raise the average $^{87}Sr/^{86}Sr$ of the upper 500 m of ocean crust by ~0.0017[58,63] with only minor increases in deep portions of the slab. For the unaltered seamount ocean crust component, we use an $^{87}Sr/^{86}Sr$ of 0.7026[23]. Complete modeling results and parameters are available in Online Supplement Table S1 and S2.

References

1 Dasgupta, R. & Hirschmann, M. M. The deep carbon cycle and melting in Earth's interior. *Earth and Planetary Science Letters* **298**, 1-13, doi:10.1016/j.epsl.2010.06.039 (2010).

2 Huybers, P. & Langmuir, C. Feedback between deglaciation, volcanism, and atmospheric CO2. *Earth and Planetary Science Letters* **286**, 479-491, doi:10.1016/j.epsl.2009.07.014 (2009).

3 Sleep, N. H. & Zahnle, K. Carbon dioxide cycling and implications for climate on ancient Earth. *Journal of Geophysical Research: Planets* **106**, 1373-1399, doi:10.1029/2000je001247 (2001).

4 Werner, C. *et al. Carbon Dioxide Emissions from Subaerial Volcanic Regions: Two Decades in Review*. 188-236 (Cambridge Univesrity Press 2019).

5 Fischer, T. P. *et al.* The emissions of CO(2) and other volatiles from the world's subaerial volcanoes. *Sci Rep* **9**, 18716, doi:10.1038/s41598-019-54682-1 (2019).

6 Gorman, P. J., Kerrick, D. M. & Connolly, J. A. D. Modeling open system metamorphic decarbonation of subducting slabs. *Geochemistry, Geophysics, Geosystems* **7**, doi:10.1029/2005gc001125 (2006).

7 Johnston, F. K. B., Turchyn, A. V. & Edmonds, M. Decarbonation efficiency in subduction zones: Implications for warm Cretaceous climates. *Earth and Planetary Science Letters* **303**, 143-152, doi:10.1016/j.epsl.2010.12.049 (2011).

8 Kelemen, P. B. & Manning, C. E. Reevaluating carbon fluxes in subduction zones, what goes down, mostly comes up. *Proc Natl Acad Sci U S A* **112**, E3997-4006, doi:10.1073/pnas.1507889112 (2015).

9 Shaw, A. M., Hilton, D. R., Fischer, T. P., Walker, J. A. & Alvarado, G. E. Contrasting He–C relationships in Nicaragua and Costa Rica: insights into C cycling through subduction zones. *Earth and Planetary Science Letters* **214**, 499-513, doi:10.1016/s0012-821x(03)00401-1 (2003).

10 de Moor, J. M. *et al.* A New Sulfur and Carbon Degassing Inventory for the Southern Central American Volcanic Arc: The Importance of Accurate Time-Series Data Sets and Possible Tectonic Processes Responsible for Temporal Variations in Arc-Scale Volatile Emissions. *Geochemistry, Geophysics, Geosystems* **18**, 4437-4468, doi:10.1002/2017gc007141 (2017).

11 Barry, P. H. *et al.* Forearc carbon sink reduces long-term volatile recycling into the mantle. *Nature* **568**, 487-492, doi:10.1038/s41586-019-1131-5 (2019).

12 Aiuppa, A., Fischer, T. P., Plank, T. & Bani, P. CO2 flux emissions from the Earth's most actively degassing volcanoes, 2005-2015. *Sci Rep* **9**, 5442, doi:10.1038/s41598-019-41901-y (2019).

13 Lopez, T. *et al.* Tracking carbon from subduction to outgassing along the Aleutian-Alaska Volcanic Arc. *Sci Adv* **9**, eadf3024, doi:10.1126/sciadv.adf3024 (2023).

14 Freundt, A. *et al.* Volatile (H2O, CO2, Cl, S) budget of the Central American subduction zone. *International Journal of Earth Sciences* **103**, 2101-2127, doi:10.1007/s00531-014-1001-1 (2014).

15 Muller, R. D. *et al.* Evolution of Earth's tectonic carbon conveyor belt. *Nature* **605**, 629-639, doi:10.1038/s41586-022-04420-x (2022).

16 Farsang, S. *et al.* Deep carbon cycle constrained by carbonate solubility. *Nat Commun* **12**, 4311, doi:10.1038/s41467-021-24533-7 (2021).

17 Li, K., Li, L., Aubaud, C. & Muehlenbachs, K. Efficient Carbon Recycling at the Central-Northern Lesser Antilles Arc: Implications to Deep Carbon Recycling in Global Subduction Zones. *Geophysical Research Letters* **47**, doi:10.1029/2020gl086950 (2020).

18 Mather, T. A. *et al.* A reassessment of current volcanic emissions from the Central American arc with specific examples from Nicaragua. *Journal of Volcanology and Geothermal Research* **149**, 297-311, doi:10.1016/j.jvolgeores.2005.07.021 (2006).

19 Bekaert, D. V. *et al.* Subduction-Driven Volatile Recycling: A Global Mass Balance. *Annual Review of Earth and Planetary Sciences* **49**, doi:10.1146/annurev-earth-071620-055024 (2020).

20 Aster, E. M. *et al.* Reconstructing CO2 concentrations in basaltic melt inclusions using Raman analysis of vapor bubbles. *Journal of Volcanology and Geothermal Research* **323**, 148-162, doi:10.1016/j.jvolgeores.2016.04.028 (2016).

21 Plank, T. & Manning, C. E. Subducting carbon. *Nature* **574**, 343-352, doi:10.1038/s41586-019-1643-z (2019).

22 Syracuse, E. M., van Keken, P. E. & Abers, G. A. The global range of subduction zone thermal models. *Physics of the Earth and Planetary Interiors* **183**, 73-90, doi:10.1016/j.pepi.2010.02.004 (2010).

23 Herbrich, A. *et al.* Cocos Plate Seamounts offshore NW Costa Rica and SW Nicaragua: Implications for large-scale distribution of Galápagos plume material in the upper mantle. *Lithos* **212-215**, 214-230, doi:10.1016/j.lithos.2014.10.014 (2015).

24 Aubouin, J. A., J. & Demant, Alain & Rangin, C. & Tardy, M. & Tournon, J. The Middle American Trench in the geological framework of Central America. doi:10.2973/dsdp.proc.67.141.1982 (1982).

25 Plank, T. & Langmuir, C. H. The chemical composition of subducting sediment and its consequences for the crust and mantle. *Chemical Geology* **145**, 325-394, doi:10.1016/s0009-2541(97)00150-2 (1998).

26 Patino, L. C., Carr, M. J. & Feigenson, M. D. Local and regional variations in Central American arc lavas controlled by variations in subducted sediment input. *Contributions to Mineralogy and Petrology* **138**, 265-283, doi:10.1007/s004100050562 (2000).

27 Sadofsky, S. *et al.* Geochemical variations in the Cocos Plate subducting beneath Central America: implications for the composition of arc volcanism and the extent of the Galápagos Hotspot influence on the Cocos oceanic crust. *International Journal of Earth Sciences* **98**, 901-913, doi:10.1007/s00531-007-0289-5 (2008).

28 Heydolph, K. *et al.* Along and across arc geochemical variations in NW Central America: Evidence for involvement of lithospheric pyroxenite. *Geochimica et Cosmochimica Acta* **84**, 459-491, doi:10.1016/j.gca.2012.01.035 (2012).

29 Plank, T., Balzer, V. & Carr, M. Nicaraguan volcanoes record paleoceanographic changes accompanying closure of the Panama gateway. *Geology* **30**, doi:10.1130/0091-7613(2002)030<1087:Nvrpca>2.0.Co;2 (2002).

30 Solomon, E. K., Miriam & Robertson, Gretchen. Data Report: Barium Cycling at the Costa Rica Convergent Margin. *Proceedings of the Ocean Drilling Program: Scientific Results* **205**, doi:10.2973/odp.proc.sr.205.210.2006 (2006).

31 Bekaert, D. V. *et al.* High (3)He/(4)He in central Panama reveals a distal connection to the Galapagos plume. *Proc Natl Acad Sci U S A* **118**, doi:10.1073/pnas.2110997118 (2021).

32 Gazel, E. *et al.* Plume–subduction interaction in southern Central America: Mantle upwelling and slab melting. *Lithos* **121**, 117-134, doi:10.1016/j.lithos.2010.10.008 (2011).

33 Reagan, M. K., Morris, j. D., Herrstrom, E. A. & Murrell, M. T. Uranium series and beryllium isotope evidence for an extended history of subduction modification of the mantle below Nicaragua. *Geochimica et Cosmochimica Acta* **58**, 4199-4212, doi:10.1016/0016-7037(94)90273-9 (1994).

34 van Keken, P. E., Wada, I., Abers, G. A., Hacker, B. R. & Wang, K. Mafic High-Pressure Rocks Are Preferentially Exhumed From Warm Subduction Settings. *Geochemistry, Geophysics, Geosystems* **19**, 2934-2961, doi:10.1029/2018gc007624 (2018).

35 Turner, S. J. *et al.* Boron isotopes in Central American volcanics indicate a key role for the subducting oceanic crust. *Earth and Planetary Science Letters* **619**, doi:10.1016/j.epsl.2023.118289 (2023).

36 Wyllie, P. & Boettcher, A. Liquidus phase relationships in the system CaO-CO2-H2O to 40 kilobars pressure with petrological applications. *American Journal of Science* **267**, 489-508 (1969).

37 Hermann, J. & Spandler, C. J. Sediment Melts at Sub-arc Depths: an Experimental Study. *Journal of Petrology* **49**, 717-740, doi:10.1093/petrology/egm073 (2008).

38 Spandler, C. & Pirard, C. Element recycling from subducting slabs to arc crust: A review. *Lithos* **170-171**, 208-223, doi:10.1016/j.lithos.2013.02.016 (2013).

39 Sisson, T. W. & Kelemen, P. B. Near-solidus melts of MORB + 4 wt% H2O at 0.8–2.8 GPa applied to issues of subduction magmatism and continent formation. *Contributions to Mineralogy and Petrology* **173**, doi:10.1007/s00410-018-1494-x (2018).

40 Snyder, G., Poreda, R., Hunt, A. & Fehn, U. Regional variations in volatile composition: Isotopic evidence for carbonate recycling in the Central American volcanic arc. *Geochemistry, Geophysics, Geosystems* **2**, n/a-n/a, doi:10.1029/2001gc000163 (2001).

41 Hilton, D. R., Fischer, T. P. & Marty, B. Noble Gases and Volatile Recycling at Subduction Zones. *Reviews in Mineralogy and Geochemistry* **47**, 319-370, doi:10.2138/rmg.2002.47.9 (2002).

42 Elliott, T. in *Inside the Subduction Factory* 23-45 (2003).

43 Turner, S. J. & Langmuir, C. H. An alternative to the ocean crust fluid + sediment melt paradigm for arc lava geochemistry. *Science* (2024).

44 Morris, J. D., Leeman, W. P. & Tera, F. The subducted component in island arc lavas: constraints from Be isotopes and B-Be systematics. *Nature* **344**, 31-36, doi:10.1038/344031a0 (1990).

45 Leeman, W. P., Carr, M. J. & Morris, J. D. Boron geochemistry of the Central American Volcanic Arc: Constraints on the genesis of subduction-related magmas. *Geochimica et Cosmochimica Acta* **58**, 149-168, doi:10.1016/0016-7037(94)90453-7 (1994).

46 Solomon, E. A. & Kastner, M. Progressive barite dissolution in the Costa Rica forearc – Implications for global fluxes of Ba to the volcanic arc and mantle. *Geochimica et Cosmochimica Acta* **83**, 110-124, doi:10.1016/j.gca.2011.12.021 (2012).

47 Krabbenhöft, A. *et al.* Constraining the marine strontium budget with natural strontium isotope fractionations (87Sr/86Sr∗, δ88/86Sr) of carbonates, hydrothermal solutions and river waters. *Geochimica et Cosmochimica Acta* **74**, 4097-4109, doi:10.1016/j.gca.2010.04.009 (2010).

48 Pearce, C. R. *et al.* Reassessing the stable (δ88/86Sr) and radiogenic (87Sr/86Sr) strontium isotopic composition of marine inputs. *Geochimica et Cosmochimica Acta* **157**, 125-146, doi:10.1016/j.gca.2015.02.029 (2015).

49 Klaver, M. *et al.* Sr isotopes in arcs revisited: tracking slab dehydration using δ88/86Sr and 87Sr/86Sr systematics of arc lavas. *Geochimica et Cosmochimica Acta* **288**, 101-119, doi:10.1016/j.gca.2020.08.010 (2020).

50 Voigt, M., Pearce, C. R., Baldermann, A. & Oelkers, E. H. Stable and radiogenic strontium isotope fractionation during hydrothermal seawater-basalt interaction. *Geochimica et Cosmochimica Acta* **240**, 131-151, doi:10.1016/j.gca.2018.08.018 (2018).

51 Amsellem, E. *et al.* The stable strontium isotopic composition of ocean island basalts, mid-ocean ridge basalts, and komatiites. *Chemical Geology* **483**, 595-602, doi:10.1016/j.chemgeo.2018.03.030 (2018).

52 Skora, S. *et al.* Hydrous Phase Relations and Trace Element Partitioning Behaviour in Calcareous Sediments at Subduction-Zone Conditions. *Journal of Petrology* **56**, 953-980, doi:10.1093/petrology/egv024 (2015).

53 Carter, L. B., Skora, S., Blundy, J. D., De Hoog, J. C. M. & Elliott, T. An Experimental Study of Trace Element Fluxes from Subducted Oceanic Crust. *Journal of Petrology* **56**, 1585-1606, doi:10.1093/petrology/egv046 (2015).

54 Sadofsky, S. J., Portnyagin, M., Hoernle, K. & van den Bogaard, P. Subduction cycling of volatiles and trace elements through the Central American volcanic arc: evidence from melt inclusions. *Contributions to Mineralogy and Petrology* **155**, 433-456, doi:10.1007/s00410-007-0251-3 (2007).

55 Saginor, I., Gazel, E., Condie, C. & Carr, M. J. Evolution of geochemical variations along the Central American volcanic front. *Geochemistry, Geophysics, Geosystems* **14**, 4504-4522, doi:10.1002/ggge.20259 (2013).

56 Carr, M. J., Feigenson, M. D., Bolge, L. L., Walker, J. A. & Gazel, E. RU_CAGeochem, a database and sample repository for Central American volcanic rocks at Rutgers University. *Geoscience Data Journal* **1**, 43-48, doi:10.1002/gdj3.10 (2014).

57 Bolge, L. L., Carr, M. J., Milidakis, K. I., Lindsay, F. N. & Feigenson, M. D. Correlating geochemistry, tectonics, and volcanic volume along the Central American volcanic front. *Geochemistry, Geophysics, Geosystems* **10**, doi:10.1029/2009gc002704 (2009).

58 Turner, S. J. & Langmuir, C. H. Sediment and ocean crust both melt at subduction zones. *Earth and Planetary Science Letters* **584**, doi:10.1016/j.epsl.2022.117424 (2022b).

59 Scher, H. D., Griffith, E. M. & Buckley, W. P. Accuracy and precision of 88Sr/86Sr and 87Sr/86Sr measurements by MC-ICPMS compromised by high barium concentrations. *Geochemistry, Geophysics, Geosystems* **15**, 499-508, doi:10.1002/2013gc005134 (2014).

60 Workman, R. K. & Hart, S. R. Major and trace element composition of the depleted MORB mantle (DMM). *Earth and Planetary Science Letters* **231**, 53-72, doi:10.1016/j.epsl.2004.12.005 (2005).

61 Feigenson, M. D., Carr, M. J., Maharaj, S. V., Juliano, S. & Bolge, L. L. Lead isotope composition of Central American volcanoes: Influence of the Galapagos plume. *Geochemistry, Geophysics, Geosystems* **5**, doi:10.1029/2003gc000621 (2004).

62 Gale, A., Dalton, C. A., Langmuir, C. H., Su, Y. & Schilling, J.-G. The mean composition of ocean ridge basalts. *Geochemistry, Geophysics, Geosystems* **14**, 489-518, doi:10.1029/2012gc004334 (2013).

63 Staudigel, H., Davies, G. R., Hart, S. R., Marchant, K. M. & Smith, B. M. Large scale isotopic Sr, Nd and O isotopic anatomy of altered oceanic crust: DSDP/ODP sites417/418. *Earth and Planetary Science Letters* **130**, 169-185, doi:10.1016/0012-821x(94)00263-x (1995).

Acknowledgments

We thank Isaac Larson for use of clean lab facilities, Stephen Eyles for providing space and technical assistance with quadrupole ICP-MS analyses, and Timothy Mock for this technical assistance with TIMS analyses. This work was supported by the National Science Foundation (Grant No. 1939080).

Author information

Authors and Affiliations

Department of Earth, Climate, and Geographic Sciences, University of Massachusetts Amherst, 627 N. Pleasant St, Amherst, MA 01003
A.J. Hammerstrom

Department of Earth, Environmental, and Planetary Sciences, Washington University in St. Louis, 1 Brookings Drive, Campus Box 1169, St. Louis, MO 63105
R. Parai

Carnegie Institution for Science, Earth and Planets Laboratory, 5241 Broad Branch Road NW, Washington D.C., 20015
R.W. Carlson

Department of Earth and Atmospheric Sciences, University of Houston, 3507 Cullen Blvd, Houston, TX 77204
S.J. Turner and A.J. Hammerstrom

Author Contributions

S.J.T. and R.P. conceived of the project and acquired funding. All authors contributed to method development. A.J.H. performed column calibration experiments and conducted all sample preparation of unknowns and conducted TIMS analysis with R.W.C. A.J.H. and S.J.T primarily contributed to data interpretation; all authors participated in data discussion. A.J.H. wrote the manuscript with input from all authors.

Ethics declarations

Competing interests

The authors declare no competing interests

Figures

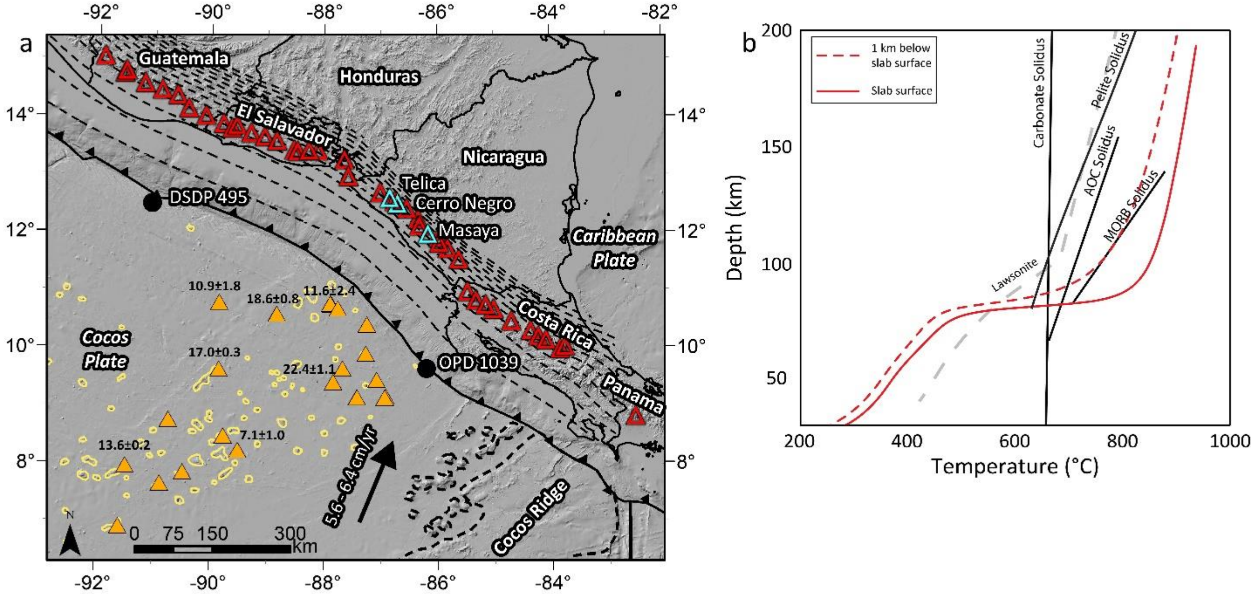

Figure 1. Map of Central American Volcanic Arc and phase diagram of Nicaraguan slab thermal profiles. **A** Open red triangles are Arc front volcanoes. Open blue triangles are volcanoes analyzed in this study. Cocos plate seamounts outlined in yellow. Solid orange triangles are Cocos plate seamounts sampled by Herbrich et al. (2015). Seamounts with measured ages are labeled. Location of DSDP site 495 and ODP 1039 indicated by solid black circles. Thin black dashed lines are slab surface contours (CI = 20 km). **B** Slab thermal profiles at the surface (solid red line) and 1 km below the slab surface (dashed red line) are plotted over H_2O-saturated solidus for carbonate[36] and pelitic sediments[37], AOC[38], and MORB[39].

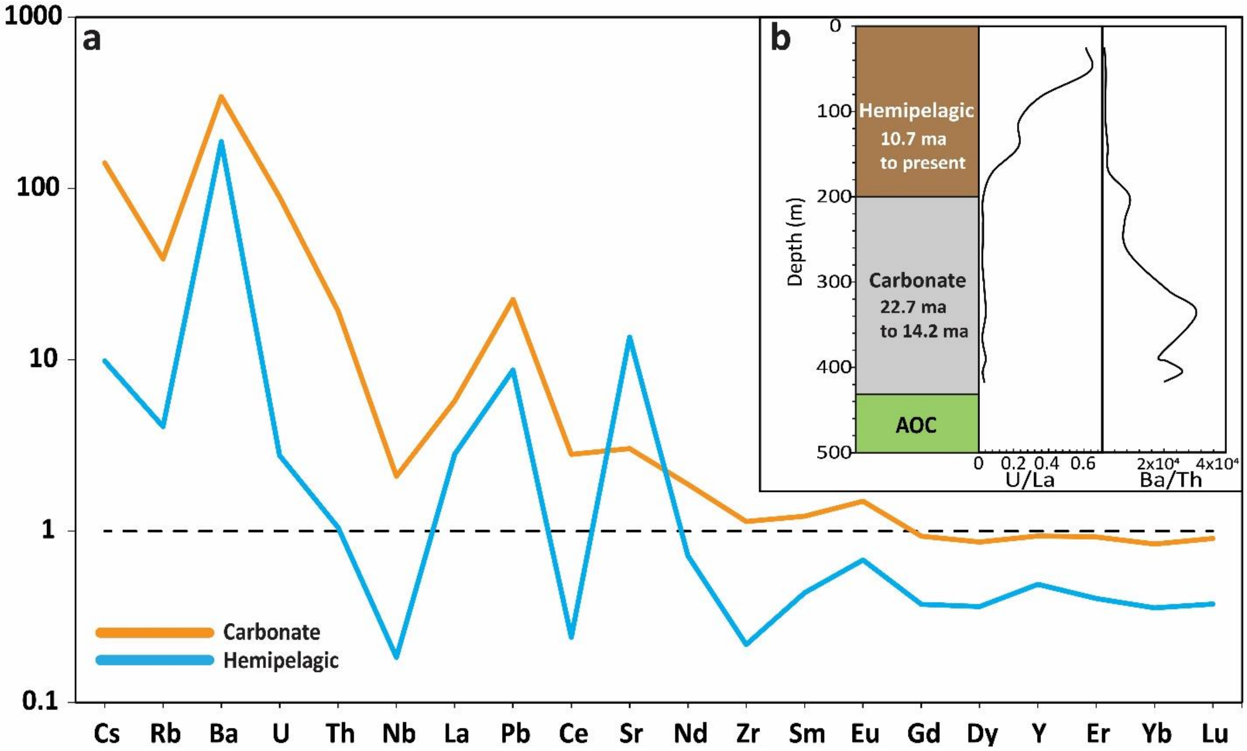

Figure 2. Compositional differences between average bulk hemipelagic and carbonate sediments from DSDP Site 495. **A** DMORB (black dotted line)[62] normalized incompatible element diagram highlighting the Bulk sediment compositions from ref 26. **B** General stratigraphy of DSDP site 495 with U/La and Ba/Th ratios vs depth (see text for explanation). A data point with an anomalously large Ba/Th value has been removed to preserve scale.

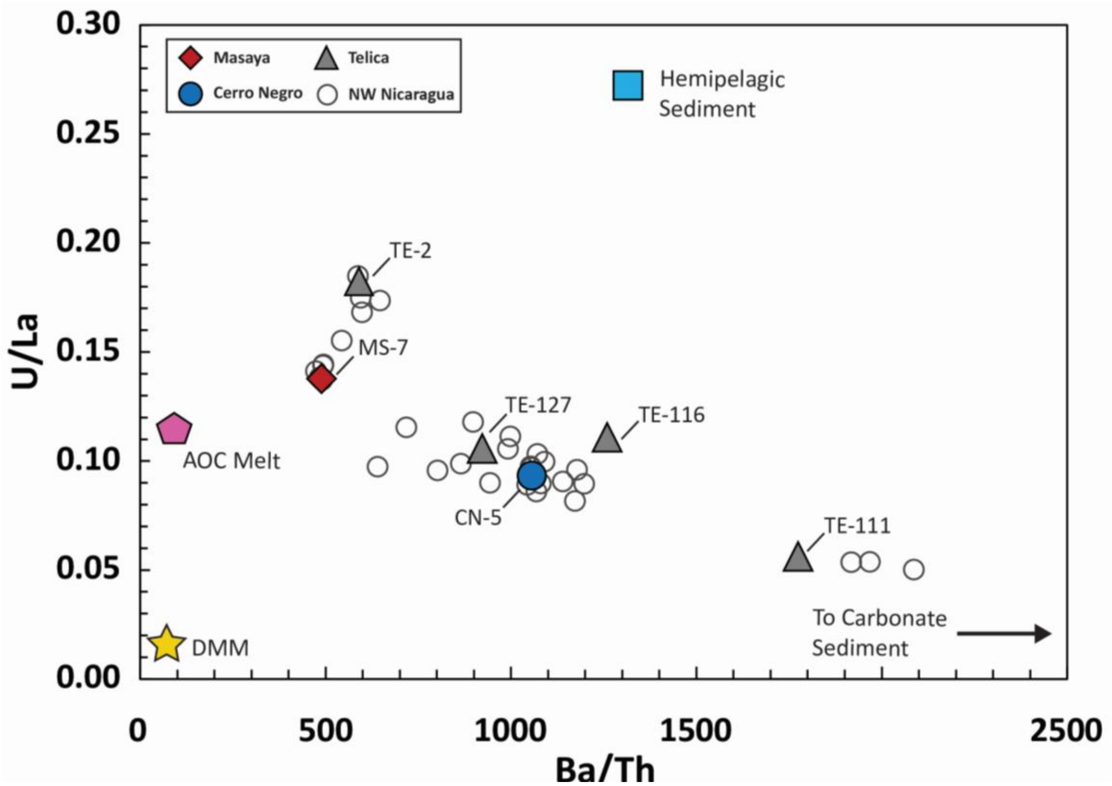

Figure 3. U/La vs Ba/Th trace element ratios showing how variations in sediment flux and the relative proportion each Cocos plate sediment influence the overall geochemical variations in Nicaraguan arc lavas (open circles). The decreasing trend of the arc lavas indicate that U/La and Ba/Th are controlled by the sediments. Volcanoes selected for this study include: Telica (gray triangles, Cerro Negro (blue circle), and Masaya (red diamond). The Blue and yellow filled squares are bulk hemipelagic and carbonate sediment compositions from ref 26, respectively. Gold star is depleted MORB mantle (DMM) of ref 60. Pink pentagon is altered ocean crust (AOC) melt.

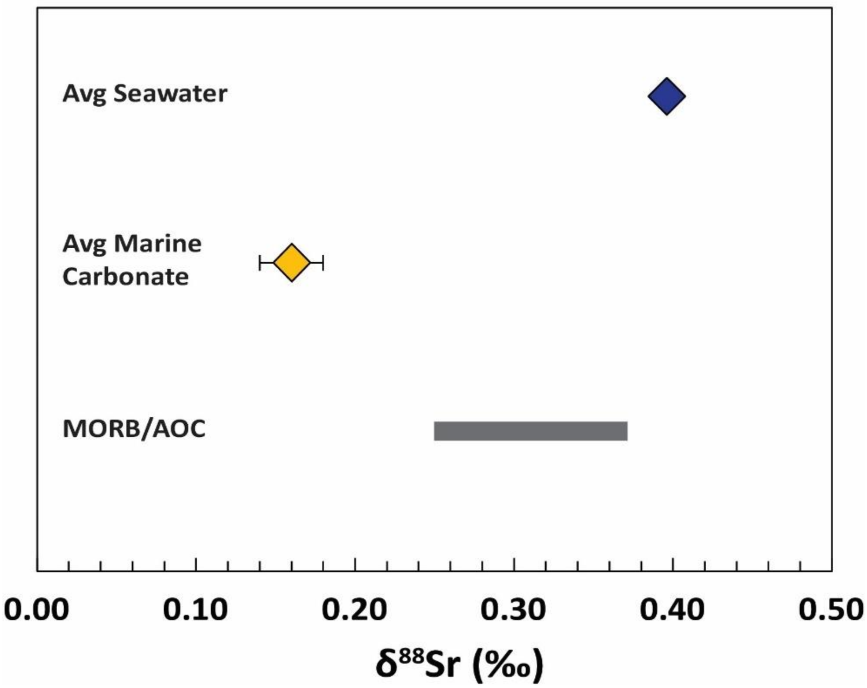

Figure 4. δ^{88}Sr of different geochemical reservoirs. Fractionation of Sr isotopes during carbonate precipitation (yellow diamond) from seawater (blue diamond) produce an average carbonate δ^{88}Sr that is significantly lighter than the reported range of δ^{88}Sr for altered and unaltered MORB (grey bar). The original δ^{88}Sr of each component transferred to the arc should not undergo discernible fractionation during magma petrogenesis therefor highlighting the Sr stable isotope system's potential to serve as a tracer for subduction components. Average seawater and marine carbonate δ^{88}Sr from ref 47 and 48. Range of MORB/AOC δ^{88}Sr from ref 49 and 50.

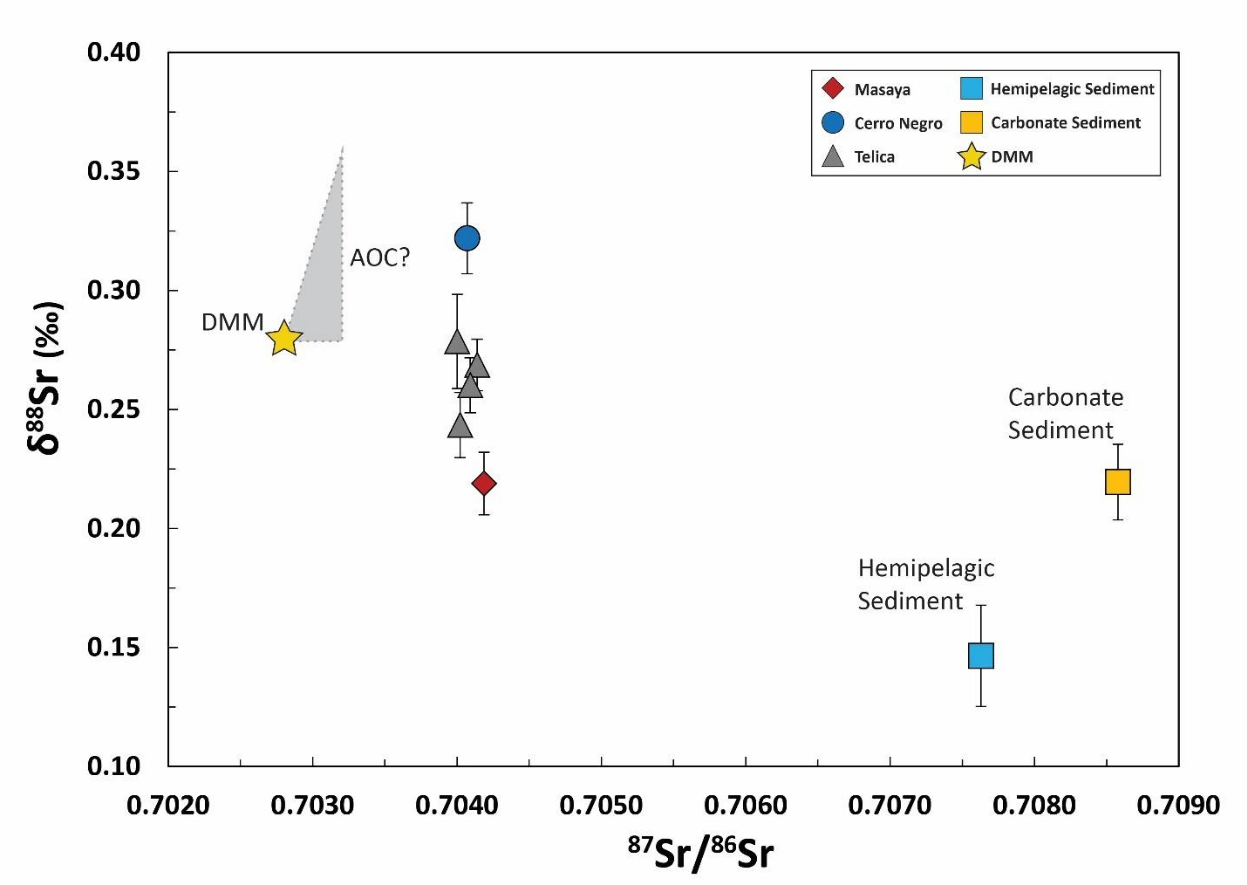

Figure 5. Three isotope plot showing Sr isotope systematics of measured Nicaraguan arc lavas and Cocos plate sediments from this study. Arc lava ^{87}Sr/^{86}Sr does not vary and falls closer to the un radiogenic slab components. Gray triangle is possible range of oceanic crustal component Sr isotope compositions based on measured and experimental δ^{88}Sr for altered and unaltered N-MORB . The upper bound of the array represents possible AOC component with a δ^{88}Sr ~0.37. This value is from experimentally altered MORB from ref 50. Gold star is ambient mantle Sr isotope composition (DMM). DMM Sr isotope values determined using average unaltered MORB δ^{88}Sr of 0.279 ± 0.05‰ from ref 49 and ^{87}Sr/^{86}Sr of 0.7028 measured in back arc basalts from La Providencia Island that have negligible subduction related trace element signatures[61].

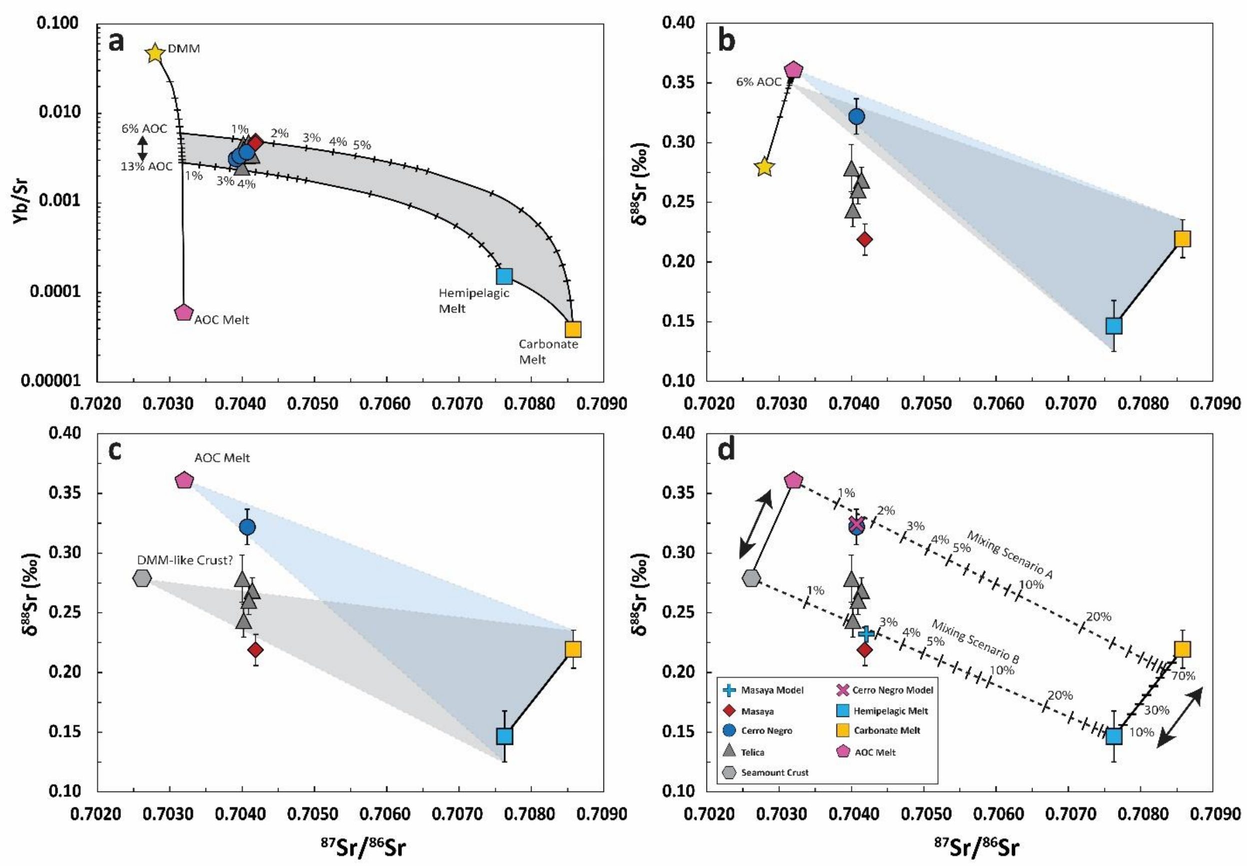

Figure 6. Plots of ^{87}Sr/^{86}Sr vs trace element ratios and δ^{88}Sr for Nicaraguan arc basalts showing binary mixing models and quantitative forward model results for Masaya and Cerro Negro volcanoes. A Yb/Sr ratio mass balance to determine relative proportion of Sr contributed from each slab component. Even at very small amounts, the mass balance indicates AOC exerts the greatest control on Nicaraguan arc magma Sr content. **B** δ^{88}Sr further highlights how AOC dominates Sr contributions. **C** A second, DMM-like, low δ^{88}Sr unaltered ocean crust component can account for the low δ^{88}Sr Masaya end member lava. **D** Strontium isotope mixing and quantitative model results. Dashed lines are mixing lines for the Cerro Negro and Masaya mixing models, respectively.

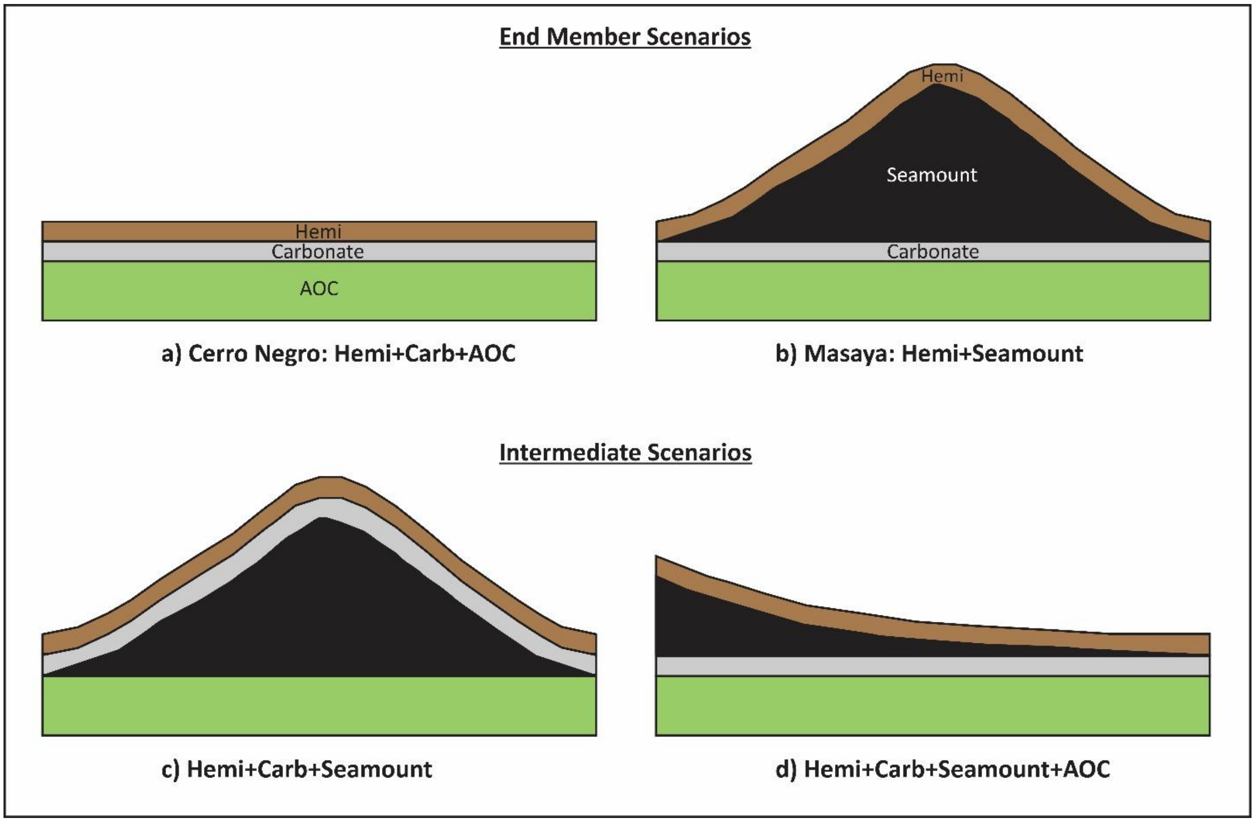

a) Cerro Negro: Hemi+Carb+AOC

b) Masaya: Hemi+Seamount

c) Hemi+Carb+Seamount

d) Hemi+Carb+Seamount+AOC

Figure 7. Conceptual models showing simplified slab surface of down going Cocos plate for several Nicaraguan subduction scenarios. A and **B** are end member scenarios for Cerro Negro and Masaya lavas, respectively. **A** reflects normal subduction in which a mixture of AOC and hemipelagic+carbonate sediments are added from the slab to the arc. In **B** large seamounts on the Cocos plate erupted after the carbonate crash effectively cap the carbonate sediments and underlying AOC. **C** and **D** represent intermediate scenarios in which various proportions of each component could reach the arc.

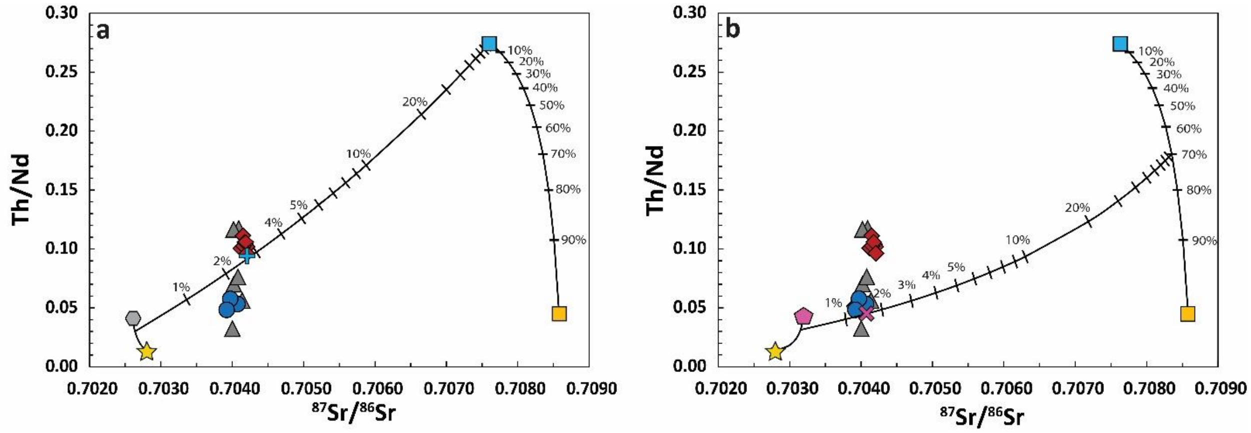

Figure 8. Plots of ^{87}Sr/^{86}Sr vs Th/Nd for Nicaraguan arc basalts showing mixing models and quantitative forward model results for Masaya and Cerro Negro volcanoes. A and **B** show Th/Nd ratio binary mixing and quantitative forward model results for Masaya and Cerro Negro end members respectively. These results are consistent with δ^{88}Sr constraints shown in **Fig. 6 A-D**. Symbols same as in **Fig. 6.** Solid hashed lines are binary mixing lines between ocean crust and sediment components.

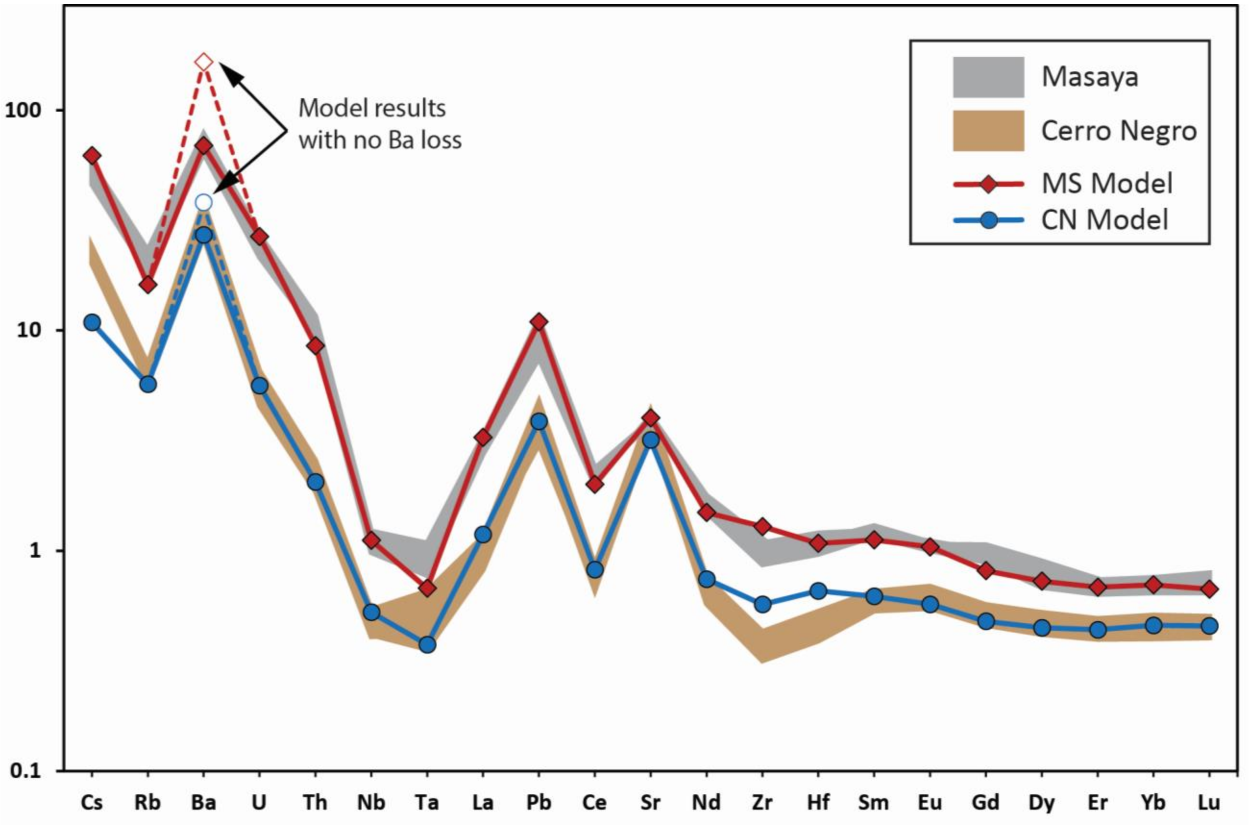

Figure 9. DMORB normalized[62] incompatible element diagram comparing modeled and measured trace element compositions for Cerro Negro and Masaya volcanoes. Shaded regions are the range of measured trace element compositions for Masya and Cerro Negro volcanoes, respectively. Dotted lines with open symbols are model results that do consider Ba loss. Following the results of ref 46 a 60% loss of Ba from the sediments in the forearc can account for the Ba mismatch in the trace element abundance model. Nb and Ta are controlled by residual rutile and not a function of slab recycling. Similarly, Zr and Hf do not match for either model, but these values are dependent on our assumption of zircon solubility in the slab melts which is not well constrained. See Turner and Langmuir (2022b) for detailed explanation on how partition coefficients for Zr, Hf, Nb, and Ta are determined.

Tables

Table 1. Strontium isotope compositions and selected trace element ratios of Nicaraguan arc basalts, Cocos plate sediments, altered ocean crust, and reference standard JB-2. δ^{88}Sr values are reported relative to SRM-987. Complete trace element compositions of for arc lavas and sediments provided in the Online Supplement.

Sample ID	Name/description	δ^{88}Sr	2SE	^{87}Sr/^{86}Sr	[Sr] ppm	Ba/Sr	Th/Nd
Arc Basalts							
CN-5	Cerro Negro	0.322	0.0149	0.704071	386.9	0.866	0.053
MS-7	Masaya	0.219	0.0131	0.704187	544.7	1.598	0.106
TE-2	Telica	0.260	0.016	0.70409	453.8	1.741	0.117
TE-116	Telica	0.269	0.024	0.70414	480.6	1.021	0.056
TE-127	Telica	0.243	0.014	0.70402	524.2	1.373	0.070
TE-111	Telica	0.279	0.020	0.70400	710.6	0.774	0.032
Sediments							
H(12R)-124m(a)	Hemipelagic	0.146	0.021	0.70758	336.2		
C(24R)-238m(a)	Carbonate	0.171	0.016	0.70881	1504.1		
C(37R)-362m(a)	Carbonate	0.219	0.016	0.70849	1		
Altered Ocean Crust							
801-MORB-11-220-FLO	ODP site 801 composite	0.247	0.008	0.70330			
801-MORB-11-220-VCL	ODP site 801 composite	0.263	0.014	0.70679			
Reference Standard							
JB-2		0.312	0.008	0.70375			

Trace element data for basalts from ref 56

Supplementary Information for 'Seamounts control subducted carbonate recycling in Central America – evidence from stable Sr isotopes', by Alexander J. Hammerstrom, Rita Parai, Richard W. Carlson, and Stephen J. Turner

Ion exchange chromatography and column chemistry calibration

Spiked and un-spiked aliquots were prepared for each unknown sample. For spiked samples, a mixed ^{87}Sr-^{84}Sr solution was added to the aliquot prior to dissolution in order to capture any mass-dependent fractionation during digestion or column chemistry. Strontium was separated using Eichrom Sr Spec resin[1] in house-made Teflon microcolumns. Resin was preconditioned by passing 3 ml of 8N Aristar Plus trace metal analysis grade HNO_3 through the columns. Next, digested sample solutions were loaded into the columns and washed twice with 3.25 ml of 8N Aristar Plus trace metal analysis grade HNO_3 to elute matrix elements (the use of 8N HNO_3 as opposed to 3N HNO_3 was required to fully separate Sr from Ba). Following the wash, purified Sr was collected by two elutions of 3 ml of Milli-Q H_2O (18.2 MΩ·cm) and evaporated until dry, then redissolved in 10 ul of 8N Aristar Plus trace metal analysis grade HNO_3. The resulting solution was then dried down once more before a final dissolution in 10 ul of 8N Aristar Plus trace metal analysis grade HNO_3.

This column procedure was calibrated to enable efficient separation of Sr from Ba and ensure complete recovery of Sr from our samples, some of which have very high Ba concentrations. The column calibration was verified using a Perkin Elmer Nexion 350D Quadrupole ICP-MS at UMass Amherst. Figure S1 shows the relative Ba and Sr concentrations of eluate collected from the sample wash, and collection phases of our final column calibration procedure using DSDP 495 sediment powder, which contains 2106 ppm Ba and 1444 ppm Sr. The total Sr yield from the collection eluant is 99.9% of the total Sr in the added solution with a negligible amount of Ba (~0.3% of the total Ba in solution passed through the column).

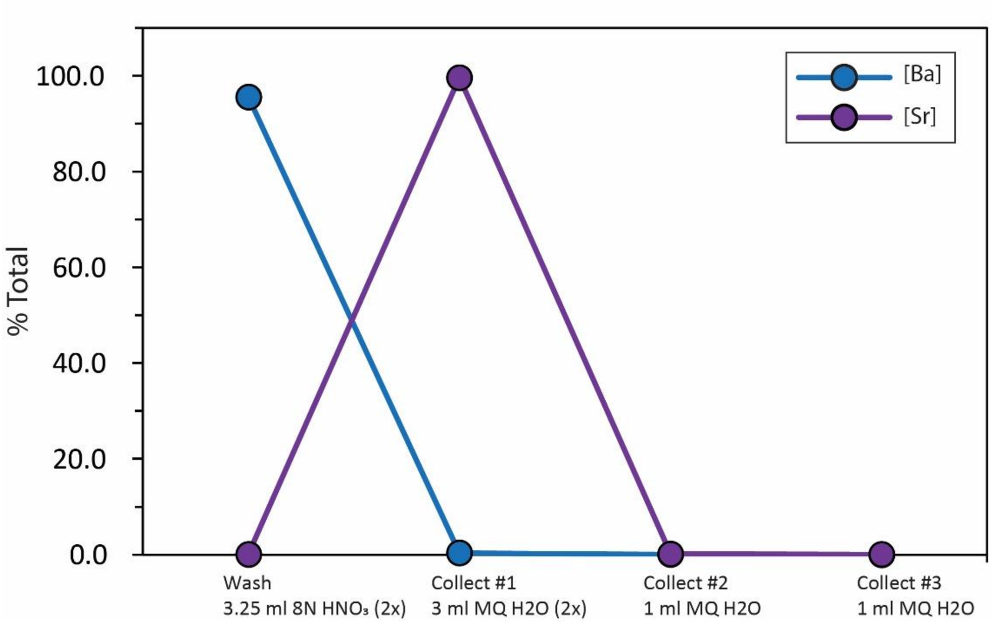

Figure S1. Sr and Ba concentrations of eluant collected from each step in our successful ion exchange chromatography column chemistry calibration experiment. Samples were measured via solution ICP-MS. Of the total Ba loaded into the column ~5% was lost during the initial column loading step (not measured) and ~95% was eluted during the wash step leaving 0.3% in the collection eluant.

TIMS analysis and data reduction

Spiked and un-spiked aliquots were analyzed for each unknown sample. For each analysis, 1ug of purified Sr was loaded onto degassed Re filaments along with a TaO_2 activator and measured using a Thermo Finnigan Triton TIMS at the Carnegie Institution for Science Earth and Planets Laboratory in Washington, D.C. ^{85}Rb was used to monitor for isobaric interference from ^{87}Rb on ^{87}Sr. In-run ^{85}Rb/^{86}Sr ratios were < 1x10^{-5} and interference corrections to the ^{87}Sr/^{86}Sr ratio were accordingly minimal. Data were acquired in 30 blocks of 20 cycles. The spike composition was verified via measurements of variable mixtures of the spike solution and SRM987 using ratios of 0:1,1:2, 1:2:,2:1,1:0. To calculate unknown Sr isotope compositions, an exponential fractionation was assumed and spike:sample mixing proportion were left as unknowns. This simple system of equations was then solved by minimizing least squares misfit using MATLAB's fminsearch solver. Results for unknowns were then normalized to fractionation-corrected SRM987 measurements (results of spiked-unspiked pairs) from the same barrel.

δ^{88}Sr measurements of ODP 801c composite samples not representative of typical altered ocean crust.

The high-δ^{88}Sr, low-^{87}Sr/^{86}Sr end member required to account for the Cerro Negro composition is consistent with altered ocean crust compositions inferred from[2], though the range of available δ^{88}Sr measurements of actual AOC samples, which are all composite samples from ODP 801c[3], does not encompass the compositional range of AOC end members required to account for the Central American arc data. The 801c site is probably not a good general proxy for AOC, however, because the upper 100 m consists of off-axis lavas rather than typical ocean crust. For example, Pockalny and Larson (2003) suggest that the presence of thick, massive, and laterally extensive off-axis lava flows could seal the original fractured ocean crust from seawater alteration. Moreover, crustal accretion models show that lava flows extending ~2-4 km off-axis can influence crustal subsidence and cause crust to fracture less extensively, decreasing the extent and depth of hydrothermal alteration[4-6]. The unique geology at site 801c may thus explain the lack of heavy δ^{88}Sr compositions observed in most of the 801c composite

AOC powders. While additional measurements of AOC samples from other localities are needed to further elucidate the variability of AOC δ^{88}Sr, the experimental data and our new arc lava δ^{88}Sr measurements suggest that typical altered oceanic crust may commonly have elevated δ^{88}Sr, and without this, there is no possible mixing solution capable of accounting for the composition of Cerro Negro.

Tables

Table S1. Quantitative forward model end member starting compositions and bulk partition coefficients.

	DMM and AOC melt compositions			Sediment melting partition coefficients, bulk sediment and modeled sediment melt compositions				
	[1]DMM	[2]AOC Melt (CN)	[2]AOC Melt (MS)	[3]Bulk Carb	[3]Bulk Hemi	[2]Sed D values	[4]Sed Melt (CN)	[4]Sed Melt (MS)
Rb	0.05	9.09	6.13	4.28	45.81	0.70	20.71	56.67
Cs	0.00	0.12	0.08	0.15	2.21	0.10	1.40	4.02
Sr	7.66	571.28	414.61	501.37	369.79	0.25	805.38	644.78
Ba	0.56	96.87	65.28	2145.48	2108.18	0.40	3353.39	3312.37
Ti	0.07	0.00	0.00	0.03	0.52	1.00	0.17	0.52
Nb	0.15	0.73	1.04	0.44	5.13	1.33	3.36	4.20
Ta	0.01	0.04	0.07	0.00	0.00	1.33	0.00	0.00
Zr	5.08	62.00	111.00	20.16	117.04	1.80	32.07	76.24
Hf	0.13	2.14	2.68	0.00	0.00	1.20	0.00	0.00
La	0.19	3.71	4.78	8.78	23.34	0.83	14.77	26.22
Ce	0.55	10.57	13.48	2.40	32.64	0.90	12.27	34.91
Nd	0.58	8.46	10.58	6.79	22.90	1.60	8.30	16.36
Sm	0.24	2.01	2.42	1.45	5.23	2.20	1.43	2.89
Eu	0.10	0.47	0.56	0.82	2.45	2.80	0.59	1.10
Gd	0.36	0.96	1.04	1.65	5.21	4.00	0.89	1.71
Dy	0.51	0.35	0.37	1.99	5.98	9.00	0.49	0.92
Er	0.35	0.10	0.10	1.40	3.84	16	0.19	0.34
Yb	0.37	0.06	0.06	1.18	3.40	50	0.05	0.10
Lu	0.06	0.01	0.01	0.19	0.53	75	0.01	0.01
Y	3.33	0.00	0.00	16.22	39.55	0.00	42.22	71.91
Sc	16.50	0.00	0.00	2.63	15.05	0.00	11.56	27.37
Pb	0.02	1.97	1.54	3.70	11.12	0.50	8.59	16.13
Th	0.01	0.37	0.44	0.16	3.35	0.60	1.50	4.49
U	0.00	0.33	0.33	0.15	3.54	0.40	1.83	5.56
δ^{88}Sr	0.279	0.36	0.279	0.22	0.15		0.20	0.15
^{87}Sr/^{86}Sr	0.7028	0.7032	0.7026	0.70858	0.70763		0.70835	0.70763

[1] Values from Workman and Hart (2005)

[2] AOC melt and sediment partition coefficients are determined in the model based on temperature input parameters following the methods described by Turner and Langmuir (2022b). Cerro Negro (CN) and Masaya (MS) AOC melt compositions correspond to "moderate" and "hot" values from Turner and Langmuir (2022b), respectively. Sediment partition coefficients correspond to "hot" values from Turner and Langmuir (2022b)

[3] Values from Patino et al. (2000). Bulk hemipelagic sediment values are average composition of the bottom three hemipelagic layers recovered from DSDP 495 (see text for details).

[4] Sed melts calculated using aggregate fractional melting equation, Sed Melt= $(D_{sed}/F_{sed})*(1-F_{sed})^{(1/D)}$, with a melt fraction of F = 0.55

Table S2. Input parameters and results for Cerro Negro and Masaya quantitative forward models.

Sample	Cerro Negro	Masaya
Input parameters		
P	1.9	1.9
F	0.22	0.15
%Carb	0.7	0
%Sed	0.0156	0.027
%AOC	0.09	0.075
Sed T (℃)	900	900
AOC T (℃)	850	900
Model Results		
Rb	5.99	16.94
Cs	0.17	0.96
Sr	352.96	444.70
Ba	310.65	789.35
Nb	1.26	2.68
Ta	0.06	0.11
Zr	52.80	119.17
Hf	1.52	2.49
La	3.70	10.20
Ce	8.21	20.06
Nd	7.03	14.11
Sm	2.06	3.71
Eu	0.69	1.26
Gd	2.12	3.59
Dy	2.45	3.99
Er	1.52	2.36
Yb	1.52	2.32
Lu	0.23	0.33
Y	18.37	39.89
Pb	1.65	4.65
Th	0.32	1.33
U	0.31	1.47
δ^{88}Sr	0.324	0.237
^{87}Sr/^{86}Sr	0.7041	0.7042

References

1 Philip Horwitz, E., Chiarizia, R. & Dietz, M. L. A novel strontium-selective extraction chromatographic resin. *Solvent Extraction and Ion Exchange* **10**, 313-336, doi:10.1080/07366299208918107 (1992).

2 Voigt, M., Pearce, C. R., Baldermann, A. & Oelkers, E. H. Stable and radiogenic strontium isotope fractionation during hydrothermal seawater-basalt interaction. *Geochimica et Cosmochimica Acta* **240**, 131-151, doi:10.1016/j.gca.2018.08.018 (2018).

3 Klaver, M. *et al.* Sr isotopes in arcs revisited: tracking slab dehydration using δ88/86Sr and 87Sr/86Sr systematics of arc lavas. *Geochimica et Cosmochimica Acta* **288**, 101-119, doi:10.1016/j.gca.2020.08.010 (2020).

4 Pockalny, R. A. & Larson, R. L. Implications for crustal accretion at fast spreading ridges from observations in Jurassic oceanic crust in the western Pacific. *Geochemistry, Geophysics, Geosystems* **4**, doi:10.1029/2001gc000274 (2003).

5 Karson, J. A. *et al.* Structure of uppermost fast-spread oceanic crust exposed at the Hess Deep Rift: Implications for subaxial processes at the East Pacific Rise. *Geochemistry, Geophysics, Geosystems* **3**, doi:https://doi.org/10.1029/2001GC000155 (2002).

6 Hooft, E. Constraining crustal emplacement processes from the variation in seismic layer 2A thickness at the East Pacific Rise. *Earth and Planetary Science Letters* **142**, 289-309, doi:10.1016/0012-821x(96)00101-x (1996).

7 Workman, R. K. & Hart, S. R. Major and trace element composition of the depleted MORB mantle (DMM). *Earth and Planetary Science Letters* **231**, 53-72, doi:10.1016/j.epsl.2004.12.005 (2005).

8 Turner, S. J. & Langmuir, C. H. Sediment and ocean crust both melt at subduction zones. *Earth and Planetary Science Letters* **584**, doi:10.1016/j.epsl.2022.117424 (2022b).

9 Patino, L. C., Carr, M. J. & Feigenson, M. D. Local and regional variations in Central American arc lavas controlled by variations in subducted sediment input. *Contributions to Mineralogy and Petrology* **138**, 265-283, doi:10.1007/s004100050562 (2000).